Numerical simulation of CO₂ geological storage in saline aquifers – case study of Utsira formation

Zheming Zhang, Ramesh K. Agarwal

Department of Mechanical Engineering & Materials Science, Washington University in St. Louis, MO 63130, USA.

Abstract
CO₂ geological storage (CGS) is one of the most promising technologies to address the issue of excessive anthropogenic CO₂ emissions in the atmosphere due to fossil fuel combustion for electricity generation. In order to fully exploit the storage potential, numerical simulations can help in determining injection strategies before the deployment of full scale sequestration in saline aquifers. This paper presents the numerical simulations of CO₂ geological storage in Utsira saline formation where the sequestration is currently underway. The effects of various hydrogeological and numerical factors on the CO₂ distribution in the topmost hydrogeological layer of Utsira are discussed. The existence of multiple pathways for upward mobility of CO₂ into the topmost layer of Utsira as well as the performance of the top seal are also investigated.

Keywords: CO₂ geological storage; Numerical simulation; Saline aquifer; Utsira formation.

1. Introduction
The majority of the ever-growing electricity demand worldwide is currently satisfied by the massive construction of fossil fuel-based power plants. However, with recent concerns on CO₂ emissions from fossil fuel based (especially coal-fired) power plants, there has been major emphasis on the development of safe and economical CO₂ capture and storage technology worldwide. Although requiring a small amount of energy for the CO₂ capture, the proposed CO₂ capture processes such as oxy-fuel [1] and chemical-looping combustion [2] have made significant progress in obtaining highly concentrated pure CO₂ after combustion. On the other hand, the technology of CO₂ geological storage (CGS) appears to be less ready for practical industrial-scale carbon reduction. Among all possible carbon sinks for sequestration, deep saline aquifers are quite attractive because of their huge sequestration capacity in US and other parts of the world with relatively smaller environmental risk [3]. However, in order to fully exploit their potential for CGS, the injection strategies need to be investigated that can address the issues of both the CO₂ storage efficiency and safety along with its economic feasibility. Numerical simulations can be employed to determine these strategies before the actual deployment of large scale sequestration in saline aquifers with enormous investment. For this purpose, DOE numerical simulator TOUGH2 (Transport of Unsaturated Groundwater and Heat, version 2.0) has been widely used worldwide to determine a-priori the CO₂ storage capacity of a saline aquifer and for risk assessment [4-6]. The TOUGH2 numerical simulation package solves the unsteady multi-phase version of mass and energy balance equations of multi-component Darcy flow in porous media, with adaptive adjustment of time

step size based on the numerical residues at each iteration of the numerical solution process [4-6]. In this paper, all simulation cases have been conducted using the single-node (non-parallel) version of TOUGH2.

Numerical simulations of existing CGS projects can help in identifying the uncertainties in CGS numerical simulations due to lack of accurate information about the hydrogeological properties of the aquifer as well as can provide important insights in the flow transportation phenomena that are essential for determining good estimates of its storage capacity and environmental risk [7]. Dozens of pilot projects have been initiated worldwide for CGS in saline formations. This paper presents the numerical simulations of CO_2 geological storage in Utsira saline aquifer using TOUGH2. We have investigated the effects of various modeling and operational factors such as the reservoir temperature, pressure, permeability, porosity, the hysteresis of relative permeability and capillary pressure, geological formation topography etc. on the fate of injected CO_2 in this aquifer. Although other researchers have also addressed such topics previously [8-15], it is hoped that this work could bring some new insights as well as provide better understanding of the nature of CGS and guidelines for best practices in its deployment.

2. Numerical simulation of CGS in Utsira saline formation

The Sleipner CGS project near Norwegian coast of North Sea is probably the most well-known and successful saline aquifer CGS demonstration to date. It has the most detailed topographic description, industrial-scale injection, and long-term monitoring data available. However, major uncertainties still exist for accurate reservoir-size simulation of the Sleipner project. Simulation studies of Sleipner project can be very helpful in understanding the actual fate of in-situ CO_2 in Utsira. Utsira formation at the injection site can be identified as nine layers of sandstone sandwiched by shale [8-10]. A generalized layered Utsira model [10] and a detailed Utsira Layer #9 model [11-15] have been established based on the available seismic surveys of Utsira formation and the monitoring data of Sleipner CGS project. The generalized Utsira model is employed to provide quick approximate estimation of upward CO_2 migration flux. The detailed Layer #9 model is developed to accurately history-match the seismic images of CO_2 migration in the topmost layer in the first ten years of injection employing the numerical simulations.

2.1 Generalized Utsira model

For this simulation, Utsira formation is modeled as a cylindrical domain with 40 km in radius and 190 m in height, packed with nine layers of sand and shale as shown in Figure 1. The most important hydrogeological and numerical parameters for the simulation are summarized in Table 1. It should be noted that each hydrogeological layer consists of several layers of computational cells. Injection takes place at the bottom layer with a rate of approximately 1 million tons per year. The axisymmetric cylindrical model of Utsira formation consists of 3913 computational cells, with cell volume ranging from 3.825×10^3 m^3 to 4.05×10^9 m^3.

Evolution of CO_2 plume for 15 consecutive years since the beginning of injection is shown in Figure 2. The upside-down pyramid shaped sub-plume suggests strong secondary-sealing effect for upward CO_2 migration, due to which there is no CO_2 contact with the topmost caprock after two years of injection and very limited contact by the third year. However, in situ CO_2 migrates laterally at an overestimated rate upon reaching the caprock, failing to yield reasonable predictions of plume migration in the later years. Later simulations suggest that lack of permeability anisotropy and caprock topography could be the reason for this plume behavior.
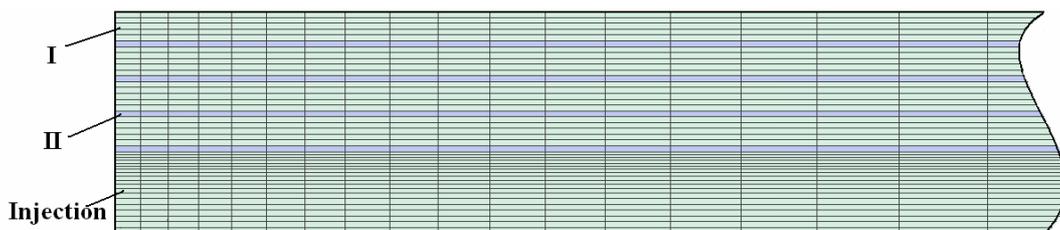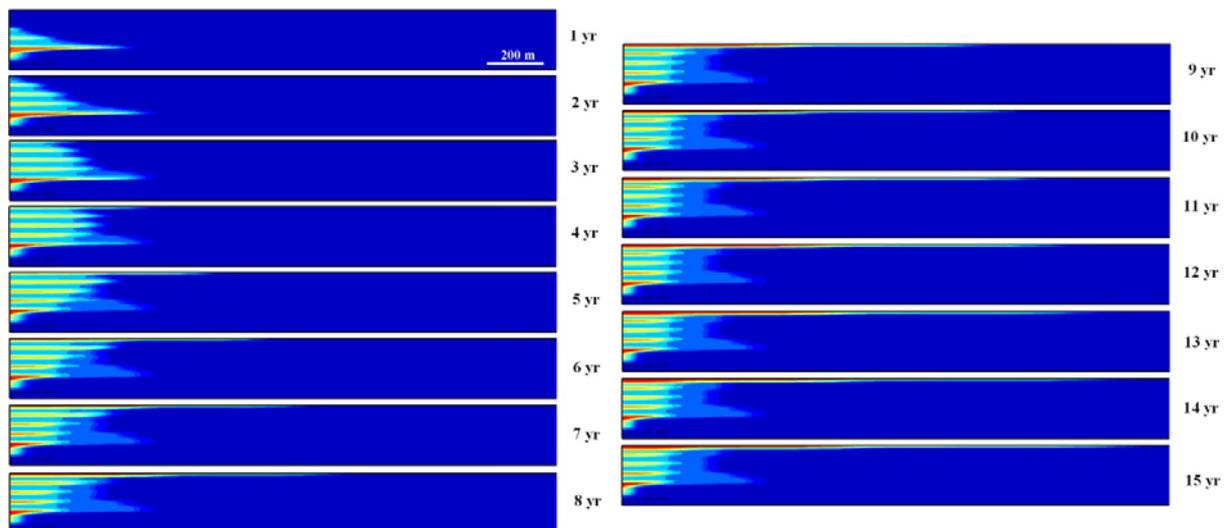

Figure 1. Generalized Utsira model illustrating its computational mesh and layered structure (I: sand, II: shale)

Table 1. Hydrogeological properties used in the generalized nine-layer Utsira model

Number of Layers (sand)	5
Number of Layers (shale)	4
Layer Thickness (sand)	Bottom layer: 70 m; other layers: 25 m
Layer Thickness (shale)	5 m
Permeability (sand)	3 Darcy
Permeability (shale)	10 mDarcy
Porosity (sand)	0.42
Porosity (shale)	0.1025
Temperature	$37^{o}C$
Pressure (bottom)	11 MPa
Injection Rate	30 kg/s
Relative Permeability	van Genuchten-Mualem
Liquid Phase Residual Saturation	0.2
Supercritical Phase Residual Saturation	0.05
van Genuchten Exponent	0.4
Capillary Pressure	van Genuchten-Mualem
Entry Pressure	3.58 kPa

Figure 2. CO_2 footprint within the Utsira formation for 15 years since the beginning of injection

The in-situ CO_2 has strong potential to migrate upward because of buoyancy, and thus accumulate under the caprock until the capillary barrier is compromised. Previous experience has demonstrated that the accumulation of CO_2 under the caprock begins at relatively early stage compared to the entire lifespan of the entire CGS project, and this is a major concern for storage security [16]. As seen from Figure 2, the lateral extent of CO_2 plume evolves rapidly after reaching the caprock after about the third year of injection (year 1999). There is some overestimation of lateral CO_2 migration in the numerical simulation compared to the site-observed CO_2 plume; it is discussed later in the paper. The analysis presented in this paper suggests that inaccurate modeling of permeability and formation topography may be the primary cause of this overestimation. Although it may not be perfectly suitable for providing an accurate prediction of the plume migration under the caprock, the generalized Utsira model nevertheless holds great promise in determining an acceptable estimate of the accumulation of CO_2 and its tendency of migration underneath the caprock. This task is of significant importance since precautionary actions could be taken to avoid potential leakage of CO_2 based on such information. CO_2 flux analysis has been

made for the topmost sandstone layer of Utsira (hydrogeological layer #9) as shown in Figure 3. Excellent agreement is observed between the simulation and the seismic amplitudes analysis [11, 15].
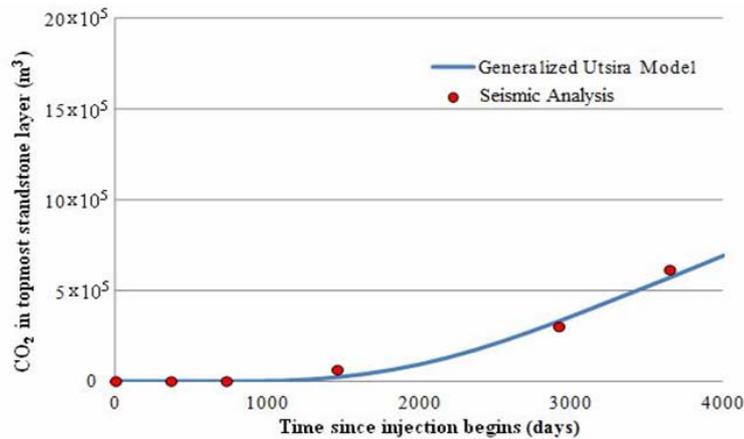

Figure 3. Supercritical CO_2 accumulation in topmost sandstone layer (Layer # 9) of Utsira formation

2.2 Detailed Utsira layer #9 model

As mentioned previously, CO_2 migration within Layer #9 describes the ultimate trapping of in- situ CO_2 and thus is of great interest. In Figure 4, field data shows striking growth in CO_2 accumulation in Layer #9 between 1999 and 2006 [11].
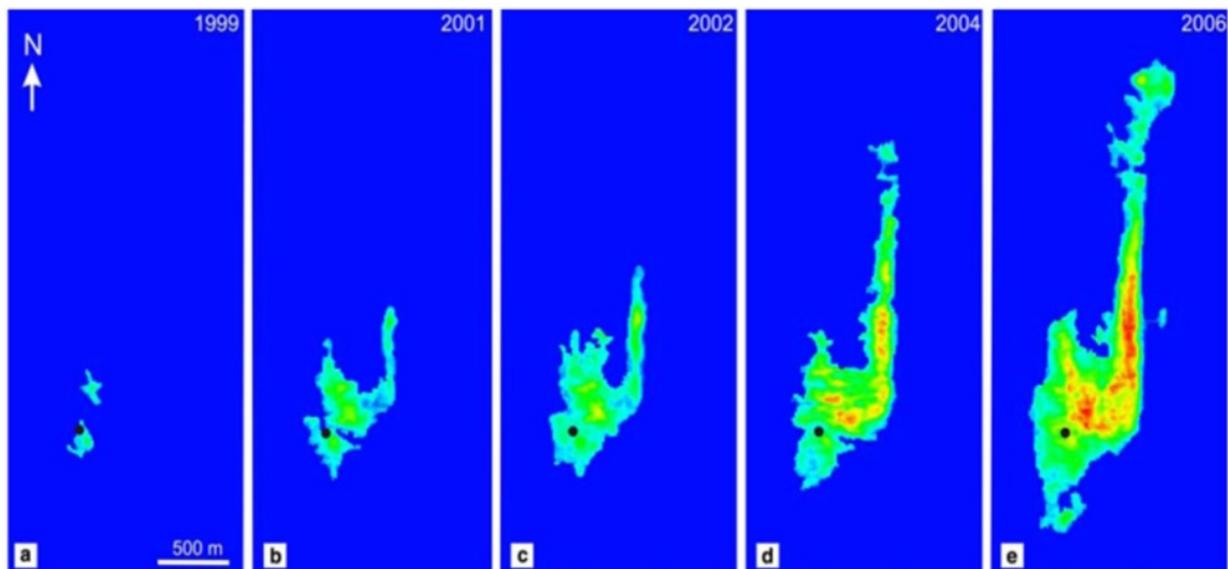

Figure 4. Amplitude maps of Layer #9: 1999 to 2006 [11]

The black dot in Figure 4 indicates the location of the injection well, which is roughly 200 m under Layer #9. Two distinct local CO_2 accumulations appear after about three years of injection (recall that injection began in 1996) indicating that CO_2 began to accumulate under the caprock. CO_2 migration under Layer #9 is not symmetric due to the topography of the caprock. The northward migration of initially accumulated CO_2 implies a local topographic dome, as seen from the "body" of the plume in Figure 4; a prominent north-tending migration implies the spill of local structurally trapped CO_2 along a north-tending topographic ridge seen as the "finger" of the plume in Figure 4. CO_2 migration along the north-tending ridge has been rather fast at about 1 m/day between 2001 and 2004 [11].

In order to examine the plume evolution within the topmost layer more closely, a 3D model of Utsira Layer #9 was created with detailed topography. Only Layer #9 and not the entire depth of Utsira was modeled because of lack of availability of detailed information for the entire Utsira formation at this

time. To ensure the accurate capture of topographic effect on plume shaping, computational domain with considerably fine mesh resolution was modeled for Layer #9 based on geological survey data. It is important to note that CO_2 has to breakthrough several layers of relatively low permeable shale prior to reaching the topmost layer. While it remains difficult to quantify the breakthrough of supercritical CO_2, the quantification of CO_2 accumulation within the topmost layer (Layer #9) is rather reliable. Therefore, a model of only the topmost layer (Layer #9) is sufficient to investigate the effect of parameters such as topography, permeability, porosity etc. on the shape of CO_2 plume.

A reservoir model with dimension of 1600 m × 4900 m with varying thickness was constructed. It covers the portion of the Utsira formation where the plume resides as shown in Figure 4. As mentioned earlier, the topography of this portion of Utsira formation can be accurately modeled based on the seismic geological survey data (provided by Zhu and Lu of Indiana University [17]) with 50 m × 50 m mesh resolution. The thickness of the computational domain varies from 3.5 m to 26.3 m with an average thickness of 11.3 m. The Layer #9 model consists of 122100 computational cells with average cell volume of about 1.024×10^5 m^3. In order to accurately capture the upward and lateral movement of accumulated CO_2, the domain is vertically discretized into 37 layers of computational cells. The topmost layer and bottom two layers represent the low permeable shale, while the 34 layers in the middle have the properties of porous sandstone. Permeability anisotropy is considered in the Layer #9 model. The topography of Layer #9 model is shown in Figure 5 and its detailed hydrogeological properties are summarized in Table 2.
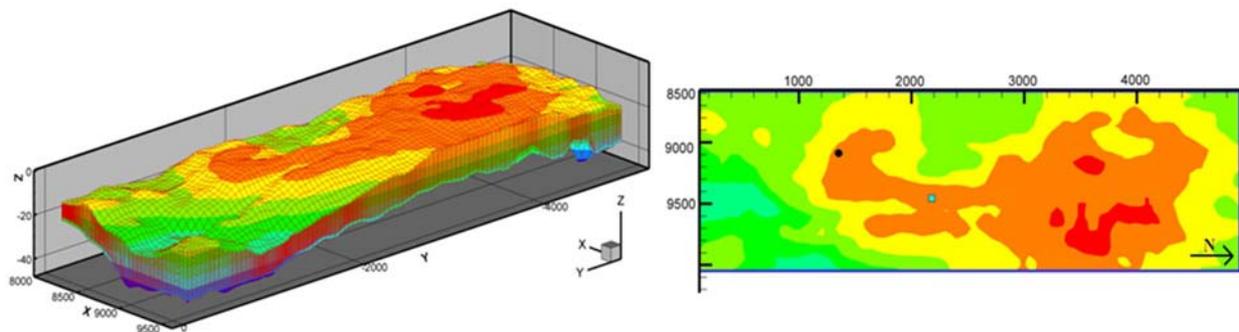

Figure 5. 3D View and plan view of Utsira layer #9 model with locations of main feeder (black dot) and secondary feeder (blue cyan square)

Table 2. Hydrogeological properties used in Utsira layer #9 model

Temperature	33° C / 36° C
Pressure	8.6 MPa
Total Utsira Formation Area	26100 km^2
Total Utsira Formation Thickness	50 m – 300 m
Layer #9 Area	1600 m × 4900 m
Layer #9 Thickness	3.5 m – 26.3m
Shale Permeability	W-E: 0.001 mDarcy, N-S: 0.001 mDarcy, Vertical: 0.0001 mDarcy
Sandstone Permeability	W-E: 2 Darcy, N-S: 10 Darcy, Vertical: 200 mDarcy
Utsira Porosity (Shale/Sandstone)	35.7 %
Residual CO_2 Saturation	0.02
Residual Brine Saturation	0.11
Relative Permeability Type	Corey/van Genuchten-Mualem
Capillary Pressure	none
Pore-Water Salinity	3.3 %
Boundary Conditions	No flow on top and bottom boundaries; Fixed state on four lateral boundaries

It should be noted that in Layer #9 model, the source of CO_2 is identified as "feeder" but not "injector" to emphasize that CO_2 is fed from lower aquifer through leakage pathways rather than by direct injection. Information on CO_2 accumulative mass has been provided by Zhu and Lu [17] and has been validated by

previous results (Figure 3) as summarized in Table 3. It can be seen that CO_2 feeding rate for Layer #9 keeps on increasing for the recorded nine years.

Table 3. Accumulative CO_2 mass in Utsira layer #9, 1999-2008

Year	Accumulative mass (kg)	Yearly feeding mass (kg)	Feeding rate (kg/s)
1999	0.00	0.00	0.00
2000	1.82×10^7	1.82×10^7	0.577
2001	5.52×10^7	3.70×10^7	1.17
2002	9.49×10^7	3.97×10^7	1.26
2003	1.45×10^8	5.01×10^7	1.59
2004	2.13×10^8	6.80×10^7	2.16
2005	3.07×10^8	9.40×10^7	2.98
2006	4.34×10^8	1.27×10^8	4.03
2007	6.03×10^8	1.69×10^8	5.36
2008	8.20×10^8	2.17×10^8	6.88

Recalling the observed secondary-sealing effect in the previous simulation described in section 2.1, it is the pressure gradient between the supercritical CO_2 phase pressure in the lower aquifer and the capillary pressure in the overlying shale layer that determines the breakthrough of CO_2 and its flow rate. When breakthrough first occurs, the pressure gradient facilitates the breakthrough from the equilibrium state resulting in relatively low breakthrough mass flux to Layer #9. However, as more CO_2 accumulates, the pressure gradient gradually increases and leads to increasing breakthrough mass flux. A 9-year average feeding rate of about 2.89 kg/s can be estimated from Table 3. The effect of both the 9-year average and the time-dependent feeding rate are investigated in the following simulations.

The significant northward-tending plume finger is rather surprising for regular pressure-gradient driven Darcy flow. Analysis suggests three possible explanations for the prominent north-tending CO_2 finger along the ridge; these are: (1) significantly higher permeability applied at the ridge, (2) existence of northward geological slope which enhances the buoyancy-driven migration along the ridge, and (3) existence of a secondary (or multiple) CO_2 pathway under the ridge. The hypothesis of significantly higher permeability at the ridge can be easily ruled out since no such evidence is obtained from the geological survey. Existence of geological slope of 5.8 m/km [11] has already been considered in the description of the topography of top-seal. Considering all three uncertainties mentioned above, a total of seven simulations are conducted as summarized in Table 4.

Table 4. Seven simulation runs for the Utsira layer #9 model

	Feeder(s)	Feeding rate	Boundary condition	Reservoir temperature (^{o}C)
1	Single	9-year average	Open	33
2	Single	Time-dependent	Open	33
3	Two	9-year average	Open	33
4	Two	Time-dependent	Open	33
5	Two	Time-dependent	Semi-open	33
6	Two	Time-dependent	Semi-open	36
7	Two (modified)	Time-dependent	Semi-open	36

The simulation time is set at nine years, which corresponds to the injection period of 1999~2008. CO_2 plume migration at the topmost computational layer is examined for each year. The goal is to obtain the best history matching to the field seismic images by conducing the seven simulations, and thus to provide insights on the importance of the modeling uncertainty.

In Figure 6, the CO_2 plume migration develops in a seemingly isotropic fashion at early stages. Then local migration of CO_2 along the north-tending ridge is captured in the simulations including the small amount of spill southward. However, two major issues need to be addressed (when comparing to the seismic images). First, the size of the plume is significantly large, especially for years 2000 and 2001. Second, northward CO_2 migration along the ridge, which reaches $y = 3000$ m by 2008 in the simulation, is significantly underestimated. There is over 10% underestimation compared to the 3400 m migration

captured by the seismic images. In addition, CO_2 plume appears to migrate faster along the east-west direction.
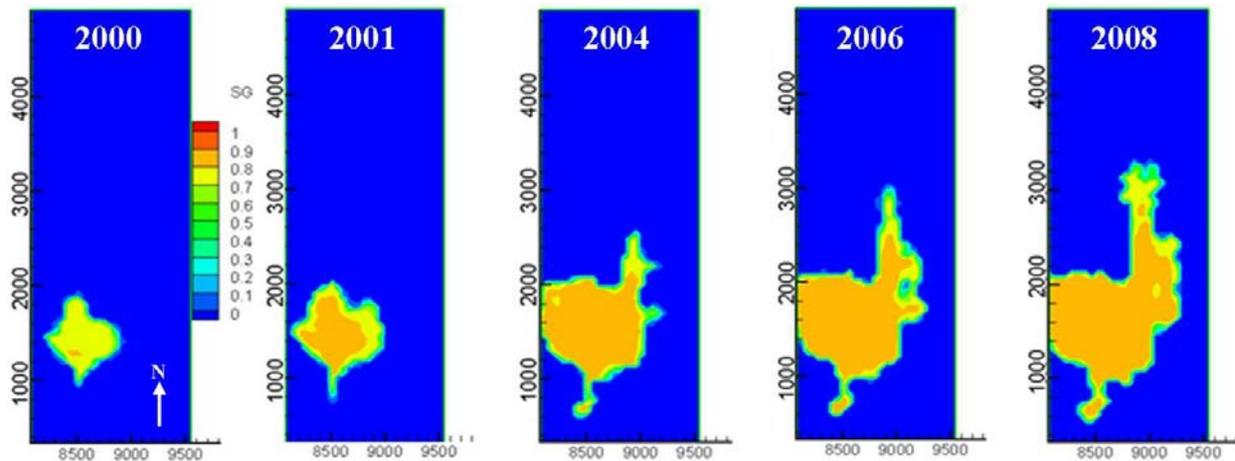

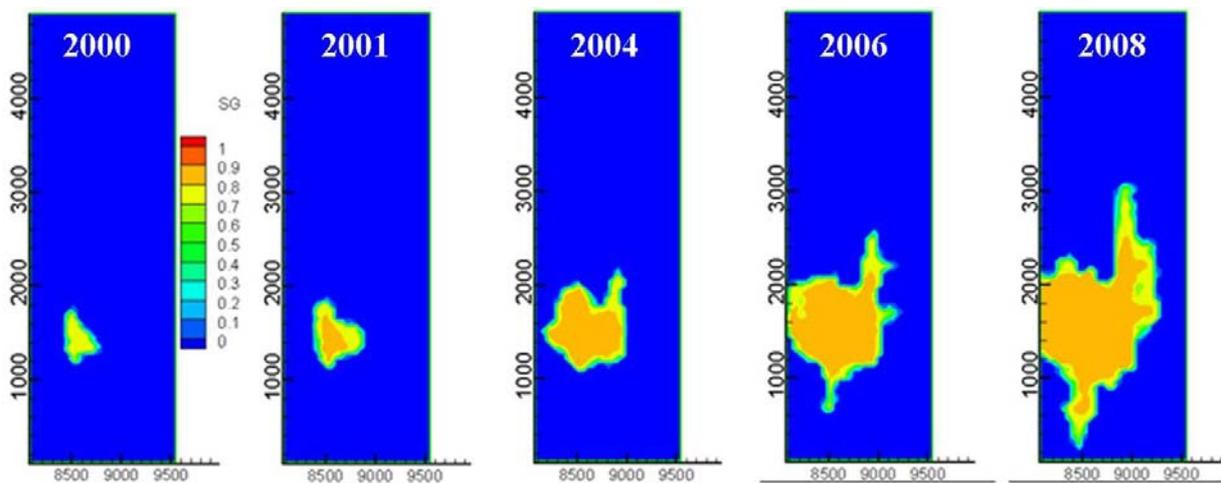Figure 6. CO_2 plume at top layer, 2000~2008, case#1

Figure 7. CO_2 plume at top layer, 2000~2008, case #2

Time-dependent CO_2 feeding scenario is introduced in the simulation shown in Figure 7. Because this is a more realistic CO_2 feeding scenario, computed plume size at early stage is greatly improved resulting in good match with the history data. However, the issue of underestimation of the northward migration of CO_2 along the ridge becomes worse, due to the lower value of the major driving force for CO_2 migration – the pressure gradient between the feeder and the ambient aquifer. Therefore, less amount of CO_2 is "pushed" to the north-tending ridge in the same time period. Although the pressure gradient gradually increases with increase in the feeding rate, the migration along the ridge is still compromised due to insufficient migration duration. Additionally, the southern CO_2 spill seems to be overestimated for year 2008. Greater east-west migration still remains.

The simulations of case #1 and case #2 imply that a single feeder is not likely to lead to sufficient plume migration along the north-tending ridge due to lack of a driving force. Since supercritical CO_2 enters Layer #9 by overcoming capillary pressure barrier of the underlying shale layer, it is generally believed that CO_2 feeding into Layer #9 is supplied by multiple possible pathways from the lower aquifers due to heterogeneity in the formation properties. Therefore, the effect of the existence of an additional feeder near the ridge is investigated. The location of the secondary feeder is set at $x = 8925$ m, $y = 2210$ m [17], as shown in Figure 5. Additionally, it is assumed that 100% of CO_2 is distributed by the main feeder during 1999 to 2001, and 85% of CO_2 is distributed by the main feeder with rest 15% distributed by the secondary feeder in 2001 and onwards.

Figure 8 gives the simulation results under the existence of two feeder scenario with 9-year average feeding rate. Compared to the results for single feeder scenarios, plume migration along the north-tending ridge for the two feeder scenario has improved as expected. However, overestimation of plume migration at early stage still occurs, as CO_2 feeding from the secondary feeder is inactive during the early stage. Additionally, the overestimation of west-east plume movement still persists.
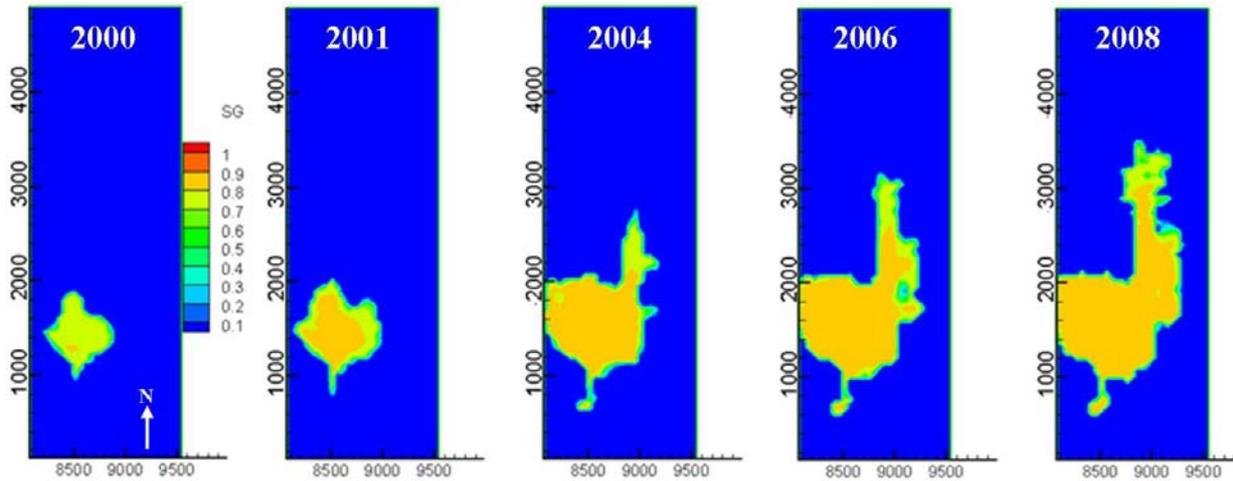

Figure 8. CO_2 plume at top layer, 2000~2008, case #3
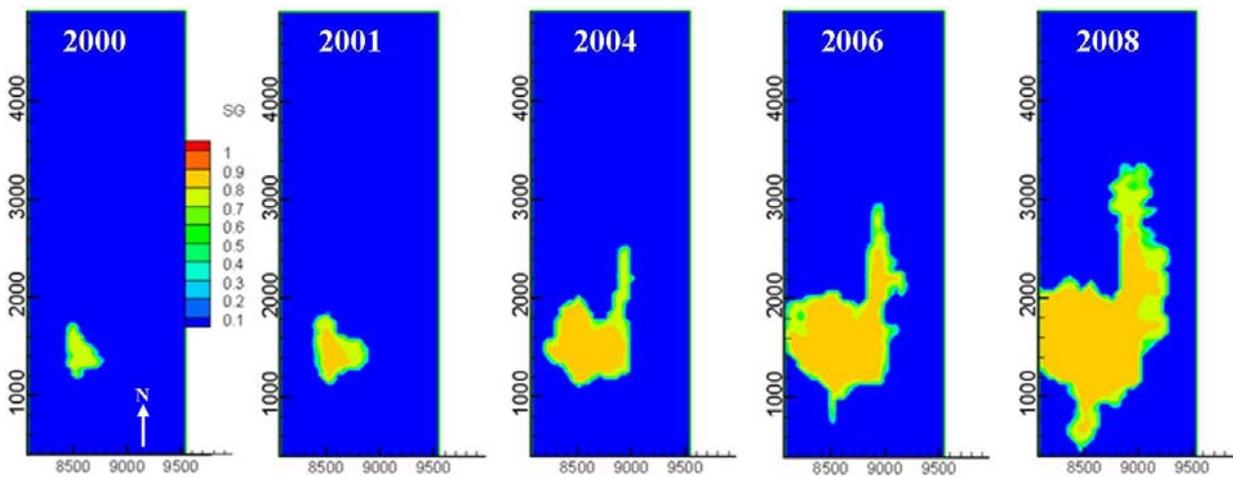

Figure 9. CO_2 plume at top layer, 2000~2008, case #4

In Figure 9, time-dependent feeding rate is applied for the two feeder scenario designated as case #4. For this case, early stage plume migration is well captured and plume migration along the north-tending ridge in later years is also improved. Nevertheless, a close comparison with the field data suggests additional work needs to be done to treat the overestimated west-east migration and further increase in the northward migration along the ridge. First, the boundary condition is modified. Closed boundary condition is applied to the western and eastern lateral boundaries, while open boundary condition is maintained at the northern and southern lateral boundaries, making the computational domain semi-open. Since the total CO_2 accumulation amount is identical, reduced migration along east-west direction will force more CO_2 to migrate along the north-south direction. Physically such semi-open boundary condition implies that CO_2 plume experiences more resistance when it migrates along the west-east direction.

As can be seen from Figure 10, the implementation of semi-open boundary condition reduces east-west plume migration effectively, and also simultaneously enhances the northward migration along the ridge. However, the simulations still do not quite match the seismic images, implying that some other important considerations in the modeling are missing.
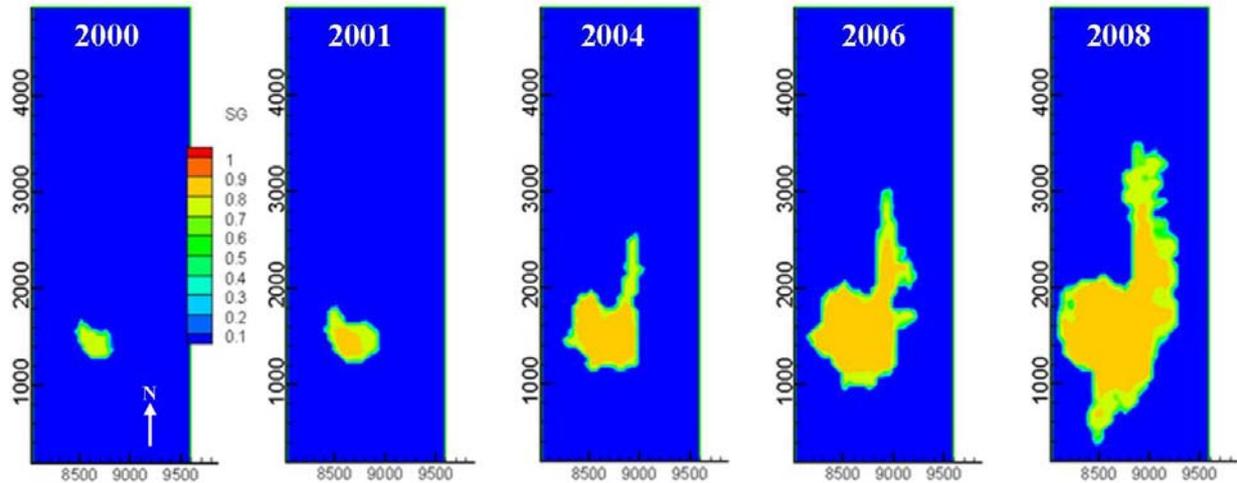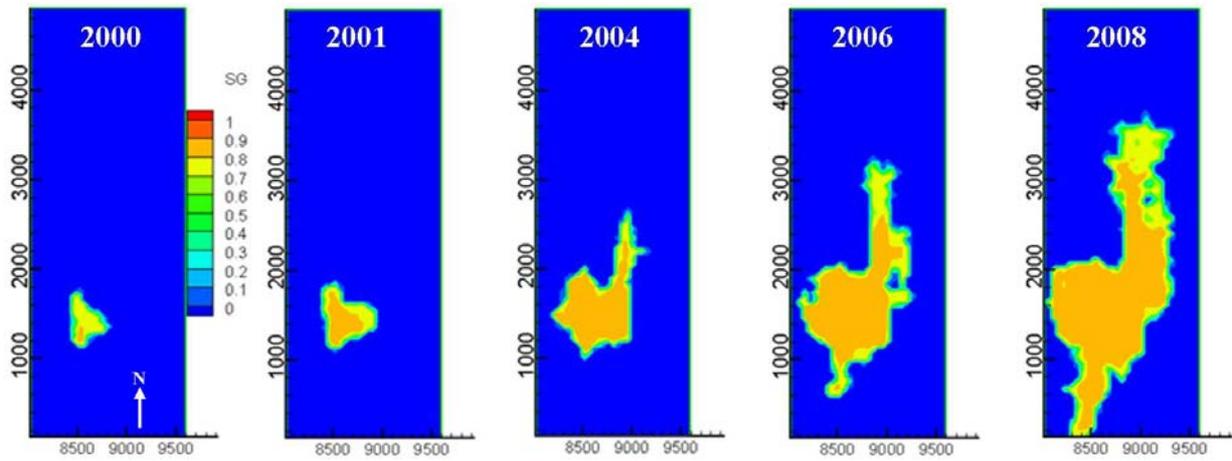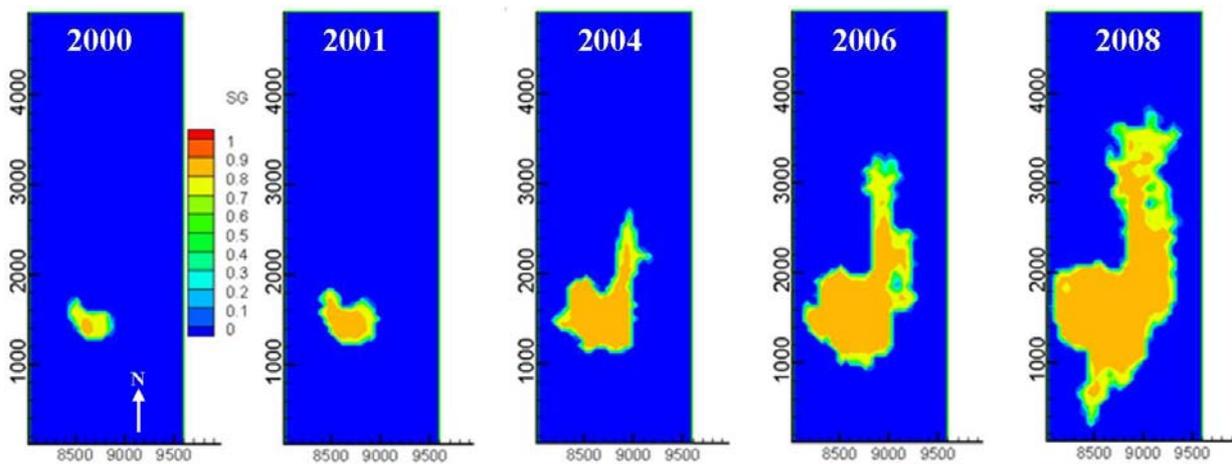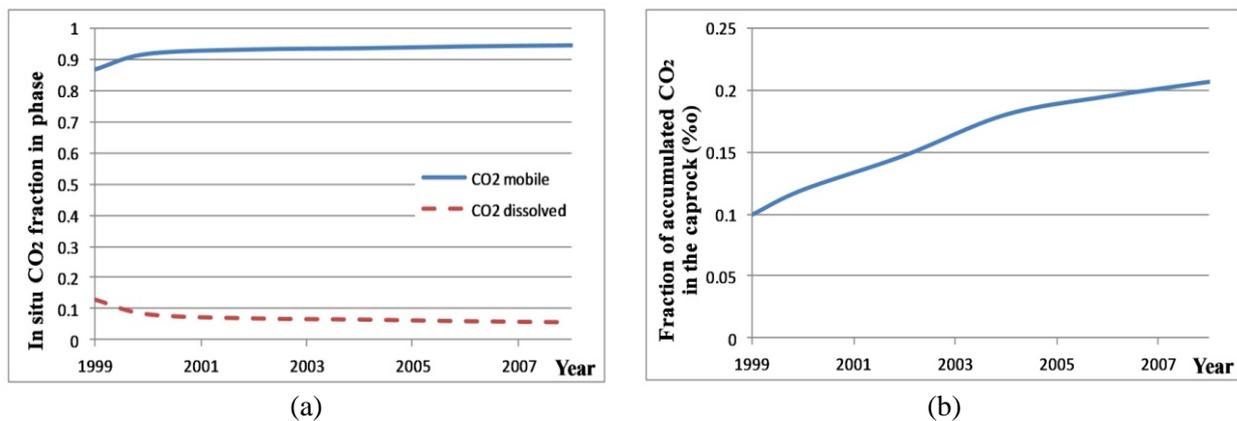
Figure 10. CO_2 plume at top layer, 2000~2008, case #5

As mentioned earlier, the only two types of driving force for plume migration are pressure gradient and buoyancy. Application of semi-open boundary condition is to essentially enhance the pressure gradient. On the other hand, a more intuitive way to enhance buoyancy is to decrease CO_2 density. In the previous simulations, given reservoir conditions led to pure supercritical CO_2 density of about 630~650 kg/m^3. However, the injected gas for Sleipner GCS project is not pure supercritical CO_2, but a 98% CO_2 and 2% methane mixture 14. Because methane is significantly lighter than CO_2, it is expected to migrate upward and concentrate in Layer #9 faster than CO_2. With the concentration of methane, it will effectively lower the density and increase the buoyancy of the CO_2-methane mixture. Since TOUGH2 does not possess the ability of modeling CO_2-methane mixture in saline aquifer, a workaround of compensating the density loss of pure CO_2 is to increase the reservoir temperature. Following Zhu's suggestion [17], the density of CO_2-methane mixture is in the range of 600 kg/m^3. Retaining other reservoir conditions the same, it requires raising the reservoir temperature by 3 ^{o}C to have CO_2 density the same as the density of CO_2 (98%) - methane (2%) mixture at actual reservoir conditions. The increased reservoir temperature causes a drop in pore-water's density and viscosity which however is negligible compared to that of CO_2. Therefore in the following simulations, reservoir temperature is increased from 33 ^{o}C to 36 ^{o}C to enhance the mobility of in-situ CO_2. It should also be noted that in Chadwick and Noy's work, the temperature of the reservoir was also numerically elevated by 3 ^{o}C in order to compensate for the methane contamination [11].

As shown in Figure 11, the increased reservoir temperature greatly enhances the plume migration in north-south direction as expected. Meanwhile, east-west migration is still confined by the semi-open boundary condition. In Figure 11, the plume shape at each year matches quite well with the corresponding seismic images. The northeast migration reaches about $y = 3300$ m in 2006, which is in the same ballpark as obtained by the seismic image. The only concern is that the southward migration still appears to be overestimated in 2008. It is possible that the increased buoyancy leads to over-spill towards south.

To treat the over-spill of CO_2 to the south after 2006, the main feeder is relocated 100 m to the east and 200 m to the north. As shown in Figure 12, CO_2 over-spill to the south is avoided by the slightly modified main feeder location. Case #7 gives satisfactory results and matches the seismic images as shown in Figure 12.

Under the model of case #7, the time-lapse in-situ CO_2 fraction in both supercritical and aqueous phases is examined as shown in Figure 13 (a). Recalling the increasing CO_2 feeding rate over time as shown in Figure 3 and Table 3, the nearly flat aqueous CO_2 fraction since year 2000 implies that the dissolution of CO_2 into the ambient brine also has strong tendency to increase, which is typically associated with the enhanced convective mixing of supercritical CO_2 and brine.

Figure 11. CO_2 plume at top layer, 2000~2008, case #6

Figure 12. CO_2 plume at top layer, 2000~2008, case #7

(a)

(b)

Figure 13. (a) CO_2 phase distribution in layer #9; (b) CO_2 accumulation in caprock

However, the overall dissolution of CO_2 in Layer #9 remains insignificant (less than 10%) for most of the time. To evaluate the leakage risk posed by the accumulation of supercritical CO_2 in Layer #9, the presence of CO_2 in the caprock is examined as shown in Figure 13(b). It is seen that the infiltration of in-situ CO_2 into the caprock only accounts for less than a quarter thousandth of the total CO_2 accumulation, which assures the performance of the caprock as an effective geological CO_2 seal.

Five major conclusions can be made from the simulations of the detailed Utsira Layer #9 model. First, it shows that the permeability anisotropy should be accurately modeled. Vertical-to-horizontal anisotropy

(vertical permeability to W-E permeability) of 1:10 has to be employed to accurately capture the upward migration of CO_2. Horizontal anisotropy (W-E permeability to N-S permeability) of 2:10 has to be employed to capture the northern spill of CO_2 into the north-tending ridge. Second, a secondary feeder is likely to exist directly under the north-tending ridge to generate sufficient plume migration along the ridge. It suggests multiple pathways for CO_2 breakthrough from the lower aquifer structure. Third, the fact that injection gas being CO_2 -methane mixture is very important in modeling since the presence of methane enhances the buoyancy. Fourth, it is critical that the time-dependent CO_2 injection is modeled. This is consistent with the behavior of CO_2 path flow breaking the capillary pressure barrier. Fifth, the simulation suggests that over 90% of CO_2 will remain in supercritical phase in Layer #9 during the injection, which is to increase the risk of caprock integrity. Finally, simulation results suggest strong mobility of supercritical CO_2 under the caprock (shale) without major leakage, implying that the caprock serves well as a non-permeable CO_2 barrier.

3. Conclusion

A well-known large scale saline formation, namely the Utsira formation, has been numerically modeled to study the CO_2 geological storage, in particular the CO_2 plume migration. The results of Utsira CGS nicely match the CO_2 migration flux data and time-lapsed seismic images for the on-going Sleipner CGS project. It suggests that the secondary-sealing effect due to the stratification of aquifer appears to be very effective in retarding the upward migration of mobile CO_2. It also reveals that caprock topography, permeability anisotropy, and contamination of injected CO_2 could all have game-changing effects on the fate of in-situ CO_2. Overall, numerical simulations of saline aquifer CGS and history-matching of the CO_2 plume evolution are challenging due to significant uncertainties in the knowledge about formation properties such as its heterogeneity and topography, and the limitations of the numerical solver in modeling and simulation. Nevertheless, once properly modeled, the numerical simulations can capture the phenomena of interest with satisfactory degree of accuracy and provide important insights into CO_2 migration and reservoir performance.

References

[1]   Buhre B.J.P., Elliott L.K., Sheng C.D., Gupta R.P., and Wall T.F. Oxy-fuel combustion technology for coal-fired power generation. Progress in Energy and Combustion Technology Science, 2005, 31 (4), pp 283-307.

[2]   He F., Li H., and Zhao Z. Advancements in development of chemical-looping combustion: a review. International Journal of Chemical Engineering, 2009, 2009, Article ID 710515, 16 pages.

[3]   US Department of Energy. 2010 carbon sequestration atlas of the United States and Canada, 3rd Edition, 2010.

[4]   Pruess K. TOUGH2: a general numerical simulator for multiphase fluid and heat flow. Lawrence Berkeley Laboratory Report LBL-29400, Berkeley, California, 1991.

[5]   Pruess K. The TOUGH codes - a family of simulation tools for multiphase flow and transport processes in permeable media. Vadose Zone Journal, 2004, 3, pp 738–746.

[6]   Pruess K., Oldenburg C., and Moridis G. TOUGH2 user's guide, version 2.0 (revised). Lawrence Berkeley Laboratory Report LBL-43134, Berkeley, California, 2011.

[7]   Class H., Ebigbo A., Helmig R., Dahle H.K., Nordbotten J.M., Celia M.A., et al. A benchmark study on problems related to CO_2 storage in geologic formations. Computational Geosciences, 2009, 13 (4), pp 409-434.

[8]   Bickle M., Chadwick A., Huppert H.E., Hallworth M., and Lyle S. Modeling carbon dioxide accumulation at Sleipner: implications for underground carbon storage. Earth and Planetary Science Letters, 2007, 255 (1-2), pp 164–176.

[9]   Chadwick R.A., Zweigel P., Gregersen U., Kirby G.A., Holloway S., and Johannessen P.N. Geological reservoir characterization of a CO_2 storage site: the Utsira sand, Sleipner, northern North Sea. Energy, 2004, 29, pp 9-10.

[10]   Audigane P., Gaus I., Czernichowski-Lauriol I., Pruess K., and Xu T. Two-dimensional reactive transport modeling of CO_2 injection in a saline aquifer at the Sleipner site. American Journal of Science, 2007, 307, pp 974-1008.

[11]   Chadwick R.A. and Noy D.J. History-matching flow simulations and time-lapse seismic data from the Sleipner CO_2 plume. in: Proceedings of 7th Petroleum Geology Conference, 2010, 7, pp 1171–1182.

[12] Arts R., Eiken O., Chadwick R.A., Zweigel P., van der Meer L., and Zinszner B. Monitoring of CO_2 injected at Sleipner using time-lapse seismic data, 2004, Energy, 29, pp 9-10.
[13] Arts R., Chadwick R.A., Eiken O., Thibeau S., and Nooner S. Ten years' experience of monitoring CO_2 injection in the Utsira sand at Sleipner, offshore Norway. First Break, 2008, 26, pp 65-72.
[14] Chadwick R.A., Arts R., Eiken O., Kirby G.A., Lindberg E., and Zweigel P. 4D seismic imaging of an injected CO_2 plume at the Sleipner field, central North Sea. Geological Society of London, Memoirs, 2004, 29, pp 311-320.
[15] Singh V., Cavanagh A., Hansen H., Nazarian B., Iding M., and Ringrose P. Reservoir modeling of CO_2 plume behavior calibrated against monitoring data from Sleipner, Norway. Society of Petroleum Engineers Annual Technical Conference and Exhibition, Florence, Italy, 2010.
[16] Zhang Z. and Agarwal R. Numerical Simulation of geological carbon sequestration in saline aquifers, three case studies. in: Proceedings of 12th Annual Conference on Carbon Capture Utilization & Sequestration, Pittsburgh, US, 2013.
[17] Zhu C. and Lu P. Personal communication. Department of Geological Sciences, University of Indiana, 2012.

Zheming Zhang is a PhD student in the department of Mechanical Engineering & Materials Science at Washington University in St. Louis, USA. He holds a B.S degree in mechanical engineering from Tsinghua University, and a M.S degree from Washington University in St. Louis. His research interests are in the applications of computational fluid dynamics and optimizations to the study of carbon capture and geological sequestration and other clean energy solutions. He is a member of NSPE, ASME, and SPE.
E-mail address: zheming.zhang@wustl.edu

Ramesh K. Agarwal received the Ph.D degree in aeronautical sciences from Stanford University, Palo Alto, CA, USA in 1975. His research interests are in the theory and applications of computational fluid dynamics to study the fluid flow problems in aerospace and renewable energy systems. He is currently the William Palm Professor of Engineering in department of Mechanical Engineering and Materials Science at Washington University in St. Louis, MO, USA. He is a Fellow of ASME, AIAA, IEEE, and SAE.
Email address: rka@wustl.edu